Research Repository UCD

Title	Outer loop control design of grid-forming converters for enhanced transient stability and current limiting capability
Authors(s)	Zhao, Xianxian, O'Donnell, Terence, Murad, Mohammed Ahsan Adib, Flynn, Damian
Publication date	2023-11-16
Publication information	Zhao, Xianxian, Terence O'Donnell, Mohammed Ahsan Adib Murad, and Damian Flynn. "Outer Loop Control Design of Grid-Forming Converters for Enhanced Transient Stability and Current Limiting Capability." Institution of Engineering and Technology, November 16, 2023. https://doi.org/10.1049/icp.2023.3217.
Conference details	Renewable Power Generation and Future Power Systems Conference 2023 (RPG 2023 UK), Glasglow, United Kingdom, 15-16 November 2023
Publisher	Institution of Engineering and Technology
Item record/more information	http://hdl.handle.net/10197/26569
Publisher's statement	This paper is a postprint of a paper submitted to and accepted for publication in Renewable Power Generation and Future Power Systems Conference 2023 (RPG 2023 UK) and is subject to Institution of Engineering and Technology Copyright. The copy of record is available at the IET Digital Library.
Publisher's version (DOI)	10.1049/icp.2023.3217

Downloaded 2026-05-01 23:36:27

The UCD community has made this article openly available. Please share how this access benefits you. Your story matters! (@ucd_oa)

© Some rights reserved. For more information

Outer Loop Control Design Of Grid-Forming Converters For Enhanced Transient Stability And Current Limiting Capability

Xianxian Zhao*, Terence O'Donnell, Mohammed Ahsan Adib Murad, Damian Flynn

School of Electrical and Electronic Engineering, University College Dublin, Belfield, Dublin, Ireland
**xianxian.zhao@ucd.ie*

Keywords: Grid-forming, virtual impedance current limiting, transient stability, droop control, dispatchable virtual oscillator.

Abstract

Current limiting is necessary to ensure the hardware integrity of grid-forming converters (GFMs), but with implications for the grid-forming ability itself. Implementing a threshold virtual impedance (TVI) is a promising current limiting technology, as it maintains the voltage source characteristic behind an impedance. In this paper, a new $\tilde{P}/f$ droop control is proposed to enhance the transient stability of a droop control-based GFM under TVI current limiting control for large fault events, which is achieved by replacing the real-time active power, P, with a modified value, $\tilde{P}$, whereby the voltage drop caused by the TVI control is not included. Existing work has demonstrated that the virtual impedance ratio, $\sigma_{X/R}^{VI}$, has a conflicting effect on system dynamics and transient stability, i.e. a small $\sigma_{X/R}^{VI}$ results in a well-damped current response, but a very limited transient stability margin, while a large $\sigma_{X/R}^{VI}$ results in a poorly-damped current response, but an acceptable transient stability margin. Under the proposed $\tilde{P}/f$ droop control, this dilemma is avoided, i.e. a small $\sigma_{X/R}^{VI}$ not only results in a well-damped current response, but also further enhances the transient stability. Finally, since the standard dispatchable virtual oscillator control (dVOC)-based GFM doesn't incorporate current limiting control, here, the same TVI current limiting control (again, a small $\sigma_{X/R}^{VI}$ is recommended for fault events) is added to the outer control loop of the original dVOC-based GFMs, such that the above $\tilde{P}/f$ droop characteristic is provided for a dVOC-based GFM.

1 Introduction

With the increasing integration of renewable energy sources, high-voltage long-distance transmission, DC grids, and power electronic (PE) converter-interfaced loads, very high PE shares are anticipated in future power systems [1]. Existing power converters are mostly controlled as "grid-following", using a phase-locked loop (PLL) to synchronise the voltage angle and frequency at the connection point, in order to precisely follow active and reactive power setpoints [2]. Since grid-following converters (GFLs) rely upon synchronisation to the grid voltage, as part of ensuring controlled and stable outputs, it follows that when the GFL share reaches a certain threshold they can no longer remain synchronised [3, 4].

Consequently, the concept of "grid-forming" is proposed. The key difference with grid-following converters is that grid-forming converters (GFMs) independently create their own internal voltage angle and frequency without relying on a PLL, by, for example, using an independent external power reference plus power feedback. One of the simplest GFM concepts mimics an ideal AC voltage source, by fixing their frequency at the rated value. Thus, GFMs can maintain their voltage angle and provide an immediate response to voltage and frequency disturbances, providing similar capabilities to synchronous generators, such as an inertial response, black-start capability and forming a voltage reference for GFLs. Consequently, GFMs are often seen as a replacement for synchronous generators in future power grids.

Due to the fast controllability of voltage source converters, GFMs without current limiting can tightly control the grid voltage, with reduced concern over system transient stability for large disturbances, assuming robust small-signal stability. However, as voltage source converters (VSCs) have much lower overcurrent ability compared to synchronous generators (typically, a VSC can only cope with double its rated current for one millisecond [5]), current limiting control is necessary to protect the converters, which greatly impacts on GFM controllability, and, hence, system transient stability.

Current limiting control techniques for GFMs can be categorised as current reference saturation, virtual impedance, and a combination of both. Saturation techniques can be implemented in different ways [6], e.g. d-axis or q-axis current reference priority, or scaling the d- and q-axis current references simultaneously. Such methods can strictly limit the GFM current, but the outer voltage control loop becomes inactive, and anti-windup techniques must be implemented for PI outer voltage control loop [6, 7]. Threshold virtual impedance (TVI) current limiting emulates the effect of an impedance when the converter current exceeds a defined value [8]. GFM voltages source behaviour, but behind an impedance, avoids the disadvantages of saturation techniques.

With the converter current being limited, the transient stability of GFMs becomes an issue for large disturbances, such as severe faults. Various control strategies, which involve slowing down changes in the GFM virtual angular speed, have been proposed to enhance transient stability under large faults, through modifying the frequency setpoint [9], reducing the active power reference [10, 11], increasing the inertial constant [12], transiently increasing the damping [13], directly freezing the angular speed to the rated or pre-fault value [6, 14], or adopting nonlinear sliding mode control [15]. However, disadvantages of these methods relate to the active power setpoint or inertial constant being changed during a fault, the active power-frequency droop characteristic not being preserved, or a switching condition being required (which may also cause mal-operation).

The major contributions of this paper are as follows:

- A simple and effective transient stability enhancement strategy for large fault events is proposed for a droop control-based GFM under TVI current limiting control, by replacing the real-time active power, P, with a modified value, $\tilde{P}$, where the voltage drop caused by TVI current limiting control is removed. Other advantages of the proposed method are that $\tilde{P} = P$ except when TVI current limiting is active (the P/f droop characteristic is retained, without affecting the power reference or inertia constant), and no switching condition is required.
- Under this new $\tilde{P}/f$ droop control, a small virtual impedance ratio $\sigma_{X/R}^{VI}$ is proposed for the TVI current limiting control, which can not only further enhance system transient stability, but also results in a well-damped current dynamic response (i.e. much smaller current peak and much less oscillations).
- The same TVI current limiting control (a small $\sigma_{X/R}^{VI}$ is recommended for fault events) is added to the outer loop of a standard dVOC-based GFM. Although the TVI current limiting control is the same, the above $\tilde{P}/f$ characteristic for a droop GFM is now incorporated for the modified dVOC-based GFM (i.e. transient stability is high).

The remainder of the paper is organised as follows: Section 2 describes the principles of droop control- and dVOC-based GFMs under the classical and proposed $\tilde{P}/f$ and TVI current limiting control. Section 3 presents the simulation results using Dymola software, and Section 4 concludes the paper.

2 Droop and Dispatchable Virtual Oscillator Control- Based Grid-Forming Converter

2.1 Classical Droop Control Based Grid-Forming Converter with Threshold Virtual Impedance Current Limiting Control

Grid-forming converters are designed to act as voltage sources instead of current sources (which is the case for grid-following inverters), and, therefore, they have the potential to replace synchronous machines (which create the voltage in today's power systems). The physical structure of a droop control based GFM and its control, as studied in this paper, are shown in Fig. 1, representing the classical structure seen in [7, 16]. The GFM is composed of a DC/AC converter (here, the DC voltage source and DC/AC converter are assumed to be ideal) and an RLC filter and transformer, while the control hierarchy consists of external cascaded voltage and current loops. In the following, essential equations relevant to the studies shown in this paper are described, with bold letters indicating vector quantities.

For classical droop control, the equations for active power and frequency, P/f, droop control are given as (1)-(4), which model the active power injected by the converter, measurement and filtering of the active power, P/f droop control, and the converter angle, respectively.

$$P = v_{od} i_{od} + v_{oq} i_{oq}, \tag{1}$$

$$\frac{dp_m}{dt} + \omega_c p_m = \omega_c P, \tag{2}$$

$$\omega_{vsm} = \omega_0 + m_p (P_{ref} - p_m), \tag{3}$$

$$\frac{1}{\omega_b} \frac{d\theta_{vsm}}{dt} = \omega_{vsm}. \tag{4}$$

The equations for the d- and q-axis output voltage references are given as (5), where Δe_d and Δe_q are the d- and q-axis voltage generated by the damping enhancement control, while $m_q \Delta Q$ is the voltage drop due to reactive power and voltage amplitude droop control (Q/V). Equations (6)(7) represent the TVI control, while (8) calculates the converter current.

$$v_{od}^* = V_{ref} + m_q \Delta Q - \Delta e_d - \Delta v_{VId}, \tag{5a}$$

$$v_{oq}^* = 0 - \Delta e_q - \Delta v_{VIq}, \tag{5b}$$

$$\Delta v_{VId} = R_{VI} i_{cd} - X_{VI} i_{cq}, \tag{6a}$$

$$\Delta v_{VIq} = R_{VI} i_{cq} + X_{VI} i_{cd}, \tag{6b}$$

$$R_{VI} = K_{pR}^{VI} \max(0, i_c - I_{nom}), \tag{7a}$$

$$X_{VI} = \sigma_{X/R}^{VI} R_{VI}, \tag{7b}$$

$$i_c = \sqrt{i_{cd}^2 + i_{cq}^2}. \tag{8}$$

Due to the fast switching characteristics of voltage source converters, the voltage and current references are perfectly followed. With this assumption, the $L_f C_f$ filter and the inner voltage and current control can be simplified as a voltage source, $v_{od}^* + j v_{oq}^*$, where v_{od}^* and v_{oq}^* are expressed as (5a) and (5b). Then Fig. 1 can be re-drawn as Fig. 2(a) in a static *abc* reference frame. It is seen in Fig. 2(a) that V_o (i.e. amplitude of $\boldsymbol{v_o}$) is less than V_{ref} when TVI current limiting control is active. The active power, P, in (1) can be written as (9) by replacing v_{od} and v_{oq} with (5a) and (5b), respectively. Here, the impacts of damping enhancement and Q/V droop control are not discussed, as they are much smaller than TVI control, due to the small coefficients and the inclusion of high-pass filters.

$$P = \left(V_{ref} + m_q \Delta Q - \Delta e_d - \Delta v_{VId}\right) i_{od} + \left(-\Delta e_q - \Delta v_{VIq}\right) i_{oq}. \tag{9}$$

In Fig. 2(a) and (9), it is seen that the active power output, P, and, hence, θ_{vsm} are impacted by the TVI current limiting control via the output current $\boldsymbol{i_o}$ and generated voltage drop

Δv_{VId} and Δv_{VIq}. In the next subsection, a simple and effective transient stability enhancement strategy is proposed, by modifying the calculation of P, as shown in Fig. 2(b).

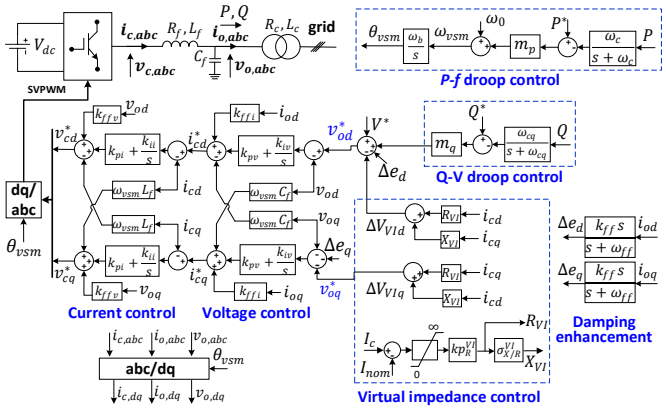

Fig. 1 Droop control-based GFM with a LCL filter, with TVI current limiting and damping enhancement control added in the outer voltage amplitude control loop.

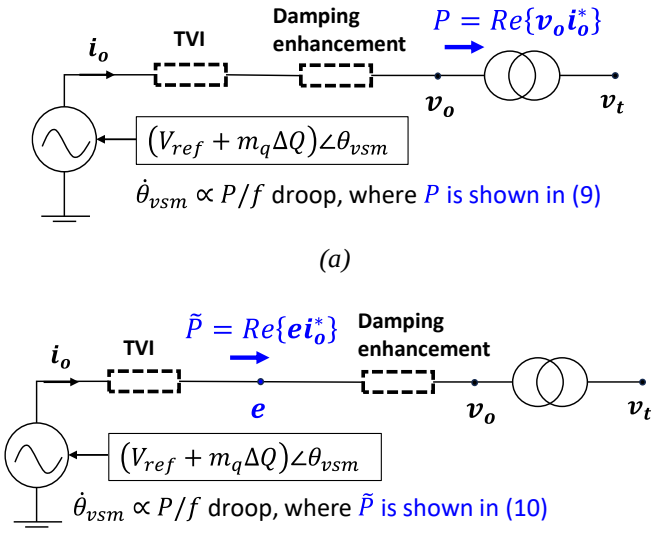

Fig. 2 Equivalent circuit of droop control-based GFM of Fig. 1 under (a) classical P/f control, and (b) proposed $\tilde{P}/f$ droop control.

2.2 Modified Droop Control Based Grid-Forming Converter for Transient Stability Enhancement

In order to enhance system transient stability under large disturbances, the active power output P in (9) is now replaced by $\tilde{P}$ in (10), for calculating the angle θ_{vsm}.

$$\tilde{P} = (V_{ref} + m_q\Delta Q - \Delta e_d)i_{od} + (-\Delta e_q)i_{oq}. \quad (10)$$

Fig. 1 is now equivalent to Fig. 2(b) under the proposed $\tilde{P}/f$ control of (10).

During steady state and small disturbances, (9) and (10) are equal, since TVI current limiting control is not active, and $\Delta V_{VI} = 0$ (ΔV_{VI} is the amplitude of the generated TVI voltage drop). During a fault, $\tilde{P} > P$ when the TVI current limiting control is active ($\Delta V_{VI} > 0$), since Δv_{VId} and Δv_{VIq} are not present in (10). Hence the increase in θ_{vsm} under the proposed droop control $\tilde{P}/f$ is smaller than that for classical droop control, P/f, which implies improved transient stability.

By directly comparing Fig. 2(a) and Fig. 2 (b), it is seen that the impacts of TVI current limiting control on θ_{vsm} are due to $\boldsymbol{i_o}$, instead of from $\boldsymbol{i_o}$ along with Δv_{VId} and Δv_{VIq}. Thus, transient stability is enhanced.

The characteristics of the proposed $\tilde{P}/f$ droop control are summarised as follows

- Calculation of $\tilde{P}$ in (10) does not require switching conditions,
- For steady state conditions and small disturbances, the active power in (9) and (10) are equivalent, and the P/f droop characteristic is retained during fault conditions.
- Equation (10) is easier to calculate compared to (9), and other aspects of the classical droop control GFM are unaffected.

2.3 Standard Dispatchable Virtual Oscillator Control Based Grid-Forming Converter

In [17], a dVOC based GFM, as shown in Fig. 3, was proposed, where the output voltage amplitude and angle are given as

$$\frac{1}{\omega_b}\begin{bmatrix}\dot{u}^*_{o\alpha}\\ \dot{u}^*_{o\beta}\end{bmatrix} = \eta\left[\left(K\begin{bmatrix}u^*_{o\alpha}\\ u^*_{o\beta}\end{bmatrix} - R(\rho)\begin{bmatrix}i_{o\alpha}\\ i_{o\beta}\end{bmatrix}\right) + \alpha\left(\frac{V^2_{ref}-V_o^{*2}}{V^2_{ref}}\right)\begin{bmatrix}u^*_{o\alpha}\\ u^*_{o\beta}\end{bmatrix}\right], \quad (11)$$

$$\theta_{vsm} = \omega_0 t + \tan^{-1}\left(\frac{u^*_{o\beta}}{u^*_{o\alpha}}\right), \quad (12)$$

$$\omega_{vsm} = \dot{\theta}_{vsm}/\omega_b, \quad (13)$$

$$v^*_{od} = V^*_o, \quad (14a)$$

$$v^*_{oq} = 0, \quad (14b)$$

where $K = \frac{1}{V^2_{ref}}R(\rho)\begin{bmatrix}P_{ref} & Q_{ref}\\ -Q_{ref} & P_{ref}\end{bmatrix}$, $V^*_o = \sqrt{u^{*2}_{o\alpha} + u^{*2}_{o\beta}}$, $R(\rho) = \begin{bmatrix}\cos(\rho) & -\sin(\rho)\\ \sin(\rho) & \cos(\rho)\end{bmatrix}$, and $\rho = \tan^{-1}\left(\frac{\omega_0 L_{line}}{R_{line}}\right)$ represents the transmission line reactance to resistance ratio.

Since (11) is based on a $\alpha\beta$ reference frame rotating at frequency ω_0, as seen in (12), a harmonic oscillator, given as $\dot{\boldsymbol{u}}^*_{o,abc} = j\omega_b\omega_0\boldsymbol{u}^*_{o,abc}$ is hidden in (11). The two bracketed terms in (11) ensure that the active and reactive power, and voltage amplitude references are followed.

Assuming $\rho = \pi/2$ (for an inductive transmission network), $V_{ref} = 1$ pu, and $Q_{ref} = 0$ pu, it is shown in [18] that in steady-state dVOC control has the same P/f and Q/V droop relationship as the droop-based GFM in Fig. 1, when $\eta = m_p$ and $1/\alpha = m_q$. However, it should be noted that their transient characteristics can be very different, especially given that dVOC has zero inertia.

2.4 dVOC-based GFM Incorporating TVI Current Limiting Control

Since current limiting control is not incorporated in the

standard design for the dVOC based GFM in [17], as seen in (11)-(14), the voltage references v_{od}^* and v_{oq}^* in (14) are included here with the same TVI current limiting and damping enhancement control as Fig. 1, which becomes (15).

$$v_{od}^* = V_o^* - \Delta e_d - \Delta v_{VId}, \tag{15a}$$

$$v_{oq}^* = 0 - \Delta e_q - \Delta v_{VIq}. \tag{15b}$$

The damping enhancement terms, Δe_d and Δe_q, are also added to (15), in order to provide fair comparison with the simulation results for droop control-based GFM in Section 3.

Although v_{od}^* and v_{oq}^* are modified, calculation of the angle θ_{vsm} is unchanged, as seen in (12), which is only based on $u_{o\alpha}^*$ and $u_{o\beta}^*$. Since $u_{o\alpha}^*$ and $u_{o\beta}^*$ are functions of the output current i_{od} and i_{oq}, instead of both the output voltage and current, θ_{vsm} for dVOC is influenced only by the output current, instead of both $\boldsymbol{i_o}$ and $\boldsymbol{\Delta v_{VI}}$. Therefore, θ_{vsm} for a dVOC GFM presents the same $\tilde{P}/f$ droop characteristic as proposed for droop-based GFMs, and thus similar transient stability enhancement is achieved.

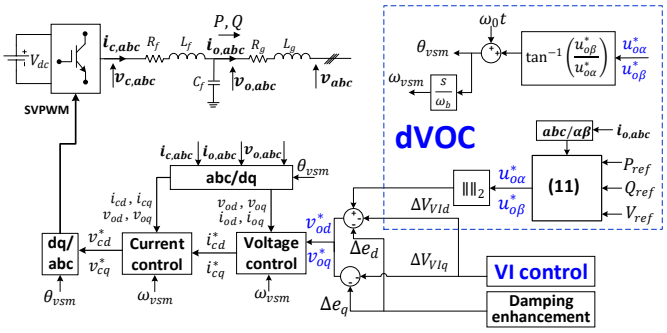

Fig. 3 Standard dVOC-based GFM [17], including proposed TVI current limiting and damping enhancement control.

2.5 Small Virtual Impedance Ratio for Droop and dVOC based GFMs under Proposed $\tilde{P}/f$ Droop Control

In [19] it was demonstrated that the virtual impedance ratio, $\sigma_{X/R}^{VI}$, has a conflicting effect on system dynamics and transient stability i.e. small $\sigma_{X/R}^{VI}$ results in a well-damped current response but a very limited transient stability margin, while large $\sigma_{X/R}^{VI}$ results in a poorly-damped current response but an acceptable transient stability margin. For the proposed $\tilde{P}/f$ droop control, this conflict disappears, i.e. small $\sigma_{X/R}^{VI}$ not only results in a well-damped current response, but also enhances the transient stability of a droop control- or dVOC-based GFM.

3 Case Studies

3.1 Validation of Proposed Droop Control-based GFMs for Transient Stability Enhancement and Current Damping

In order to show enhanced transient stability for the proposed $\tilde{P}/f$ droop control for a droop control-based GFM under TVI current limiting control, four cases are studied:

Case 1: The GFM in Fig. 1 with classical P/f droop control is connected to an equivalent AC grid with equivalent resistance and reactance of 0.02 pu and 0.2 pu (based on converter capacity base). The active and reactive power, and voltage references are given as $P_{ref} = 0.9$ pu, $Q_{ref} = 0$ pu, and $V_{ref} = 1$ pu, respectively. Other parameters are shown in Table 1, where the inner voltage and current proportional-integral controller parameters are taken from [20]. A 3-phase fault is applied at 2 s by reducing the grid voltage from 1 pu to 0.01 pu, which then recovers to 1 pu after 160 ms. Note that the virtual impedance ratio $\sigma_{X/R}^{VI} = 5$, and the maximum current limit I_{max} for calculating the TVI parameters is 1.2 pu. Further details can be found in [21].

Case 2: Same as Case 1, but the GFM now operates under proposed $\tilde{P}/f$ droop control, where $\tilde{P}$ is calculated by (10).

Case 3: Same as Case 1, but $\sigma_{X/R}^{VI}$ is reduced to 0.5, in order to demonstrate that using small $\sigma_{X/R}^{VI}$ under the original P/f droop control will result in a well-damped current response, but a very limited transient stability margin [19]. It follows that $K_{pR}^{VI} = 3.36$, based on the TVI parameters tuning principle of limiting the converter steady-state current to $I_{max} = 1.2$ pu when a bolted fault is applied at the point of common coupling [21].

Case 4: Same as Case 2, but the virtual impedance ratio is reduced from 5 to 0.5, in order to demonstrate that using a small $\sigma_{X/R}^{VI}$ under the proposed $\tilde{P}/f$ droop control can not only further improve transient stability but also make the converter current dynamics well-damped.

All simulations are performed using the Modelica language [22], as implemented using Dymola software, whereby all modelling details are completely transparent and user-created models can be easily integrated. A variable integration time step is applied, with the integration tolerance set as 0.0001.

The simulation results for Cases 1-4 are shown in Fig. 4. Fig. 4(a) shows that after the fault is cleared, for the classical P/f droop control under Case 1 the GFM is barely stable, since the active power output takes a long time (≈2.6 s) to recover to the pre-fault value. During the recovery period, the terminal voltage is as low as 0.88 pu, since the TVI is still active as the post-fault current exceeds I_{nom}, as seen in Fig. 4(d)(c). Reducing the virtual impedance ratio $\sigma_{X/R}^{VI}$ from 5 under Case 1 to 0.5 under Case 3, causes the barely stable GFM to become unstable, with the active power falling negative before recovering to the pre-fault state, as seen in Fig. 4(a). During this unstable period, the converter current is very high (1.35 pu), causing the terminal voltage to fall as low as 0.75 pu, as seen in Fig. 4(c)(d).

Comparing Case 1 with Case 2, Fig. 4(a) shows that the proposed $\tilde{P}/f$ droop control greatly improves the transient stability of the GFM, i.e. the active power recovers to pre-fault levels within ≈0.85 s with $\tilde{P}/f$ droop, instead of ≈2.55 s for the classical P/f control. Comparing Cases 2 with 4, both operating under $\tilde{P}/f$ control, Fig. 4(a) shows that transient

stability is enhanced when employing a smaller virtual impedance ratio. The result is different to that in [19], where when using the classical P/f it is seen that reducing the virtual impedance ratio reduces the transient stability margin. The reason is that in the classical P/f droop control, a smaller $\sigma_{X/R}^{VI}$ causes larger reduction of P as the resistive effect is larger. On the contrary, in the proposed $\tilde{P}/f$ droop control, the voltage drop of the TVI control is not included in the calculation of $\tilde{P}$, hence $\tilde{P}$ does not become smaller by using a reduced $\sigma_{X/R}^{VI}$, instead it becomes larger. The sub-figure in Fig. 4(c) shows that when $\sigma_{X/R}^{VI} = 0.5$, the converter peak current is lower (1.3 pu instead of 1.6 pu) with much lower oscillations, and reaches steady-state much sooner (0.5 ms instead of 15 ms), making it possible to reduce the overcurrent requirement for the voltage source converters. Fig. 4(b) shows that improving transient stability is associated with the virtual angular speed changing more slowly during the fault, which is a key principle of the proposed $\tilde{P}/f$ droop control, as described in Section 2.

Using the same simulation settings as above, additional results (not shown here) indicate that the GFM under the classical P/f droop control has a fault critical clearing time of ≈160 ms, while the equivalent duration for $\tilde{P}/f$ droop is ≈320 ms. With $\tilde{P}/f$ droop control, when reducing the virtual impedance ratio $\sigma_{X/R}^{VI}$ from 5 to 0.5, the GFM can tolerate fault durations exceeding 640 ms, and the converter current exhibits a lower peak with reduced oscillations. It follows that the proposed $\tilde{P}/f$ droop control can noticeably improve the GFM transient stability under fault events, while small $\sigma_{X/R}^{VI}$ can further improve stability with the converter current dynamics well-damped. The conclusions are not affected by the network changes (such as transmission line length or resistance and inductance ratio) or modified controls (such as increased virtual inertia for the GFM).

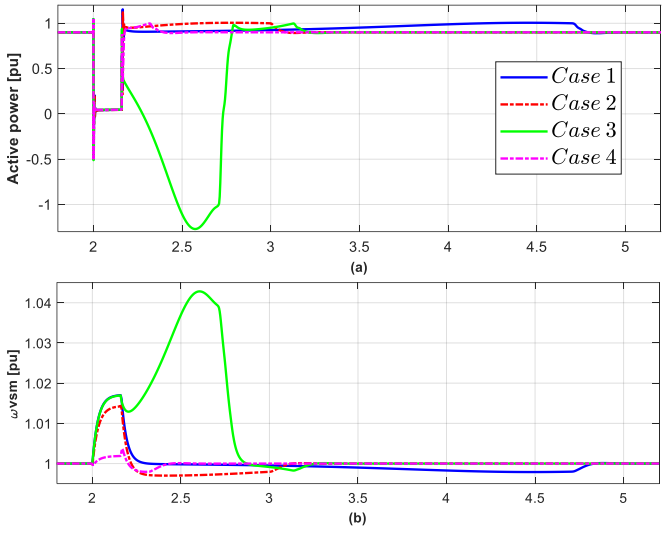

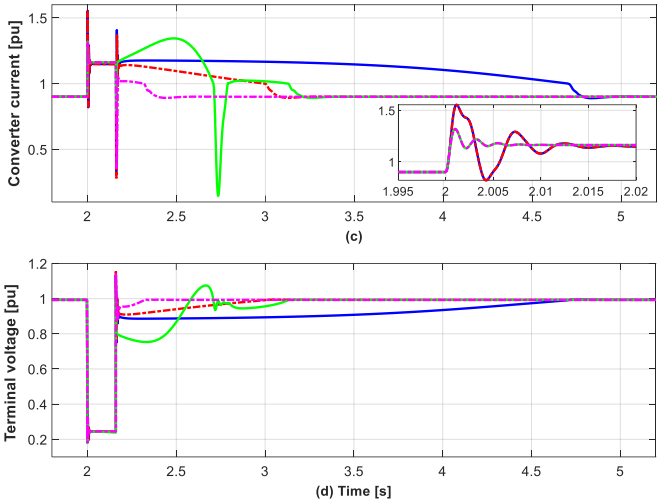

Fig. 4 Droop control-based GFM under Cases 1-4. (a) Active power output, (b) virtual angular speed, (c) converter current, and (d) the terminal voltage.

3.2 Validation of Proposed TVI Control for dVOC-based GFMs Incorporating $\tilde{P}/f$ Droop Characteristic

Case 5: The dVOC-based GFM, Fig. 3, without the proposed TVI current limiting control of (15), is connected to the same equivalent AC grid as Case 1. For comparison, Fig. 1, the droop control-based GFM without TVI current limiting control is also simulated. For both dVOC and droop GFMs, to ensure the same P/f and Q/V droop in steady-state, $Q_{ref} = 0$ pu, $V_{ref} = 1$ pu, and $\tan(\rho) = 200$ (i.e. $\rho \approx \pi/2$), $\eta = m_p$ and $1/\alpha = m_q$ are set based on the results in [18]. $P_{ref} = 0.9$ pu for both GFMs, the same as Case 1. Other parameters are shown in Table 1. The same fault as Case 1 is applied to the AC grid.

Case 6: Same dVOC GFM as Case 5, but with the proposed TVI current limiting control of (15) incorporated. $\sigma_{X/R}^{VI} = 5$, and the current limit is 1.2 pu.

Case 7: Same as Case 6, but smaller virtual impedance ratio, i.e. $\sigma_{X/R}^{VI} = 0.5$.

The simulation results for Case 5 are shown in Fig. 5, while those for Cases 6 and 7 are compared against Cases 2 and 4 in Fig. 6.

Comparing Fig. 6(a)(d) against Fig. 5(a)(d) shows that without current limiting control, the active power output and terminal voltage for both droop and dVOC GFMs are much higher than that when the converter current is limited during the fault. Moreover, the active power and terminal voltage quickly recover to pre-fault values once the fault is cleared. The result is expected, and confirms the strong controllability and robust stability of a GFM when its current is not limited. However, the overcurrent requirement is paramount, given that the inverter current is seen here to reach very high transient peak (≈5 pu) and quasi-steady-state (2.8 pu) values during the fault, as shown in Fig. 5(c).

Fig. 5(b) and Fig. 6(b) show that the virtual angular speed of the dVOC-based GFM rapidly increases to high values when the fault occurs, which may cause issues for frequency sensitive devices. In contrast, the droop control-based GFM achieves much smoother variations in angular speed, which demonstrates the consequences of the zero-inertia dVOC characteristic. Fig. 5(a)(c)(d) also shows improved damping for droop control relative to dVOC, even though the parameters are the same for the inner cascaded voltage and current control and LCL filters, and the steady-state P/f and Q/V droop characteristics are the same for both GFMs (since $\rho \approx \pi/2$, $\eta = m_p$, and $1/\alpha = m_q$).

Fig. 6 shows that by comparing Cases 2 and 6, or Cases 4 and 7, the dynamic responses of the dVOC-based GFM under TVI current limiting control are well matched to the droop control-based GFMs under the proposed $\tilde{P}/f$ droop control, which, similar to the proposed $\tilde{P}/f$ control, indicates the effectiveness of the modified dVOC-based control to enhance transient stability. Comparing Case 6 against Case 7 (using a smaller virtual impedance ratio), the active power output recovers much faster, and the post-fault terminal voltage is much higher, as seen in Fig. 6(a)(d). Fig. 6(c) also shows that the converter peak current is lower with fewer oscillations, and reaches steady-state more quickly. It can be concluded that applying a small virtual impedance ratio for dVOC GFM under TVI current limiting control can not only enhance transient stability, but can also improve the converter current dynamic responses, similar to a droop control-based GFM under the proposed $\tilde{P}/f$ droop control.

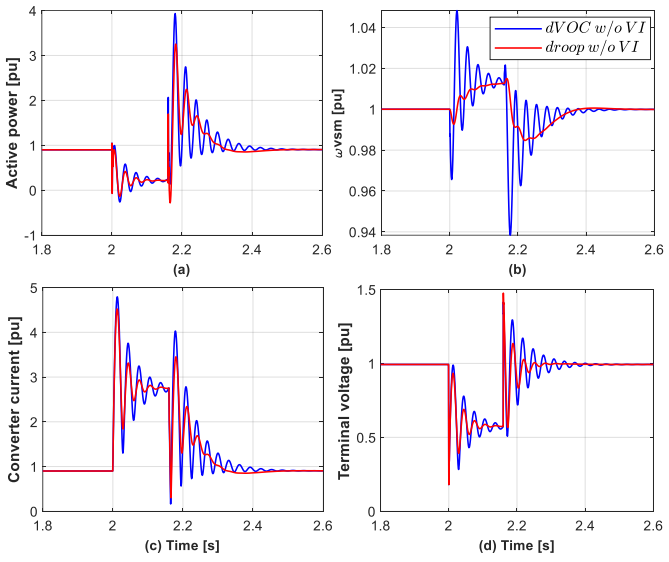

Fig. 5 dVOC and droop control-based GFMs without TVI current limiting control under Case 5. (a) Active power output, (b) virtual angular speed, (c) converter current, and (d) the terminal voltage.

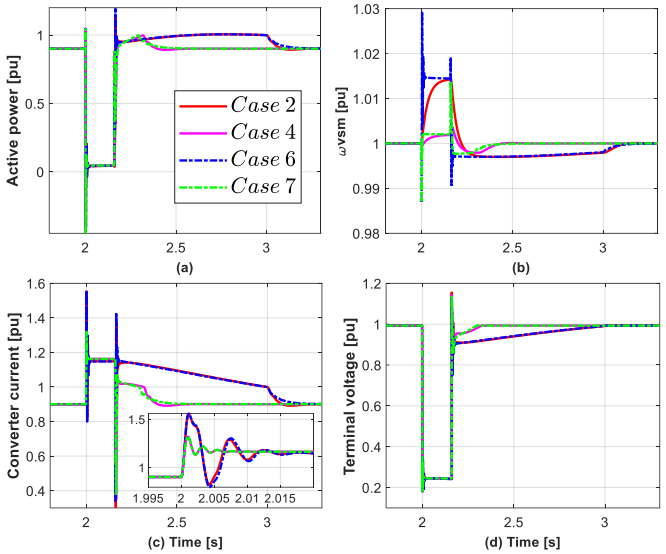

Fig. 6 dVOC-based GFM under Cases 6 and 7, along with droop control-based GFM under Cases 2 and 4. (a) Active power output, (b) virtual angular speed, (c) converter current, and (d) the terminal voltage.

Table 1 Parameters of droop control- and dispatchable virtual oscillator control-based grid-forming converters

Parameters	Values (pu)
For both droop control- and dVOC-based GFM:	
R_f, L_f, C_f	0.005, 0.15, 0.066
k_{pv}, k_{iv}, k_{pi}, k_{ii}	0.52, 1.16, 0.74, 1.19
K_{pR}^{VI}, $\sigma_{X/R}^{VI}$	0.67, 5 or 3.36, 0.5
I_{nom}	1
For droop control-based GFM:	
m_p, m_q	0.02, 0.0001
ω_{cq}	31.4 rad/s
ω_c	31.4 rad/s
For dVOC-based GFM:	
ρ	200
η, α	m_p, $1/m_q$

4 Conclusion

In order to enhance the transient stability of a droop control-based GFM with TVI current limiting control under large fault events, a new $\tilde{P}/f$ droop control has been proposed here, which replaces the active power, P, with a modified version, $\tilde{P}$, whereby the voltage drop due to TVI control is excluded. Subsequently, a small virtual impedance ratio, $\sigma_{X/R}^{VI}$, is recommended for the proposed $\tilde{P}/f$ droop control, which not only results in a well-damped current response (i.e. much lower peak and fewer oscillations), but also enhances the transient stability. In addition, since the standard dVOC-based GFM in [17] does not incorporate current limiting control, the same TVI control (small $\sigma_{X/R}^{VI}$ is again recommended for fault events) is incorporated here within the outer dVOC control loop, such that the above $\tilde{P}/f$ droop characteristic is also

provided. The effectiveness of the three proposals has been demonstrated through electromagnetic transient simulations for a range of case studies using Dymola software on a small test system.

5 Acknowledgements

The work has been supported by SEAI (Sustainable Energy Authority of Ireland) under RD&D Award 22/RDD/776.

6 References

[1] Hatziargyriou, N., Milanović, J., Rahmann, C., Ajjarapu, V., Cañizares, C., Erlich, I., Hill, D., Hiskens, I., Kamwa, I., Pal, B: 'Stability definitions and characterization of dynamic behavior in systems with high penetration of power electronic interfaced technologies', IEEE PES Tech. Rep. PES-TR77 2020.

[2] Rocabert, J., Luna, A., Blaabjerg, F., Rodriguez, P. 'Control of power converters in AC microgrids', IEEE Trans. Power Electron. 2012, 27, pp. 4734–4749.

[3] Yu, M., Roscoe, A.J., Dyśko, A., Booth, C.D., Ierna, R., Zhu, J. and Urdal, H.: 'Instantaneous penetration level limits of non‐synchronous devices in the British power system', IET Renew. Power Gener., 2017, 11(8), pp. 1211-1217.

[4] Zhao, X., Thakurta, P.G., Flynn, D. 'Grid-forming requirements based on stability assessment for 100% converter-based Irish power system', IET Renew. Power Gener. 2022, 16, pp. 447–458.

[5] Infineon Technical report, 'AN2011-05 Industrial IGBT Modules Explanation of Technical Information', November 2015.

[6] Zhao, X., Flynn, D: 'Freezing grid-forming converter virtual angular speed to enhance transient stability under current reference limiting', Proceedings of IEEE 21st Workshop Control Modeling Power Electronics Aalborg, Denmark, 2020.

[7] Bottrell, N., Green, T.C.: 'Comparison of current-limiting strategies during fault ride-through of inverters to prevent latch-up and wind-up', IEEE Trans. Power Electron., 2013, 29, pp. 3786–3797.

[8] Paquette, A.D. and Divan, D.M.: 'Virtual impedance current limiting for inverters in microgrids with synchronous generators', IEEE Trans. Ind. Appl., 2014, 51(2), pp. 1630-1638.

[9] Huang, L., Xin, H., Wang, Z., Zhang, L., Wu, K. and Hu, J.: 'Transient stability analysis and control design of droop-controlled voltage source converters considering current limitation', IEEE Trans. Smart Grid, 2017, 10(1), pp. 578-591.

[10] Qoria, T., Gruson, F., Colas, F., Denis, G., Prevost, T. and Guillaud, X.: 'Critical clearing time determination and enhancement of grid-forming converters embedding virtual impedance as current limitation algorithm', IEEE Trans. Emerg. Sel. Topics Power Electron., 2019, 8(2), pp. 1050-1061.

[11] Shuai, Z., Shen, C., Liu, X., Li, Z. and Shen, Z.J.: 'Transient angle stability of virtual synchronous generators using Lyapunov's direct method', IEEE Trans. Smart Grid, 2018, 10(4), pp. 4648-4661.

[12] Qoria, T., Rokrok, E., Bruyere, A., François, B. and Guillaud, X.: 'A PLL-free grid-forming control with decoupled functionalities for high-power transmission system applications', IEEE Access, 2020, 8, pp. 197363-197378.

[13] Xiong, X., Wu, C., Cheng, P. and Blaabjerg, F.: 'An optimal damping design of virtual synchronous generators for transient stability enhancement', IEEE Trans. Power Electron., 2021, 36(10), pp. 11026-11030.

[14] Zhao, X. and Flynn, D.: 'Grid-Forming Converter Angular Speed Freezing to Enhance Transient Stability in 100% Grid-Forming and Mixed Power Systems', IFAC-PapersOnLine, 2022, 55(9), pp. 425-430..

[15] Eskandari, M. and Savkin, A.V.: 'On the impact of fault ride-through on transient stability of autonomous microgrids: Nonlinear analysis and solution', IEEE Trans. Smart Grid, 2020, 12(2), pp. 999-1010.

[16] D'Arco, S., Suul, J.A., Fosso, O.B.: 'Automatic tuning of cascaded controllers for power converters using eigenvalue parametric sensitivities', IEEE Trans. Ind. Appl., 2014, 51, pp. 1743–1753.

[17] Colombino, M., Groß, D., Brouillon, J.S. and Dörfler, F.: 'Global phase and magnitude synchronization of coupled oscillators with application to the control of grid-forming power inverters', IEEE Trans. Autom. Contr., 2019, 64(11), pp. 4496-4511.

[18] Seo, G.S., Colombino, M., Subotic, I., Johnson, B., Groß, D. and Dörfler, F.: 'Dispatchable virtual oscillator control for decentralized inverter-dominated power systems: Analysis and experiments', Proc. IEEE Appl. Power Electron. Conf. Expo. (APEC), Anaheim, CA, USA, 2019, pp. 561–566.

[19] Taoufik, Q., Wu, H., Wang, X. and Colak, I.: 'Variable virtual impedance-based overcurrent protection for grid-forming inverters: small-signal, large-signal analysis and improvement', 2022, IEEE Trans. Smart Grid, DOI: 10.1109/TSG.2022.3232987

[20] Qoria, T., Gruson, F., Colas, F., Guillaud, X., Debry, M.S. and Prevost, T.: 'Tuning of cascaded controllers for robust grid-forming voltage source converter', Proc. Power Syst. Comput. Conf., 2018.

[21] Zhao, X. and Flynn, D.: 'Stability enhancement strategies for a 100% grid‐forming and grid‐following converter‐based Irish power system', IET Renew. Power Gener., 2022, 16(1), pp. 125-138.

[22] Fritzson, P. Principles of Object-Oriented Modeling and Simulation with Modelica 3.3: A Cyber-Physical Approach, John Wiley & Sons: Hoboken, NJ, USA, 2014.